HHS Public Access

Author manuscript

Adv Healthc Mater. Author manuscript; available in PMC 2017 January 21.

Published in final edited form as:

Adv Healthc Mater. 2016 January 21; 5(2): 255–265. doi:10.1002/adhm.201500370.

Investigation of the Viability, Adhesion, and Migration of Human Fibroblasts in a Hyaluronic acid/Gelatin Microgel-Reinforced Composite Hydrogel for Vocal Fold Tissue Regeneration

Hossein K. Heris[1], **Jamal Daoud**[2], **Sara Sheibani**[3], **Hojatollah Vali**[4], **Maryam Tabrizian**[2,4,*], and **Luc Mongeau**[1,*]

[1] Department of Mechanical Engineering, Faculty of Engineering, McGill University, Montreal (QC)

[2] Department of Biomedical Engineering, Faculty of Medicine, McGill University, Montreal (QC)

[3] Biological Threat Defence Section, Defence R&D Canada-Suffield, Medicine Hat, (AB)

[4] Faculty of Dentistry, McGill University, Montreal (QC)

Abstract

The potential use of a novel scaffold biomaterial consisting of crosslinked hyaluronic acid (HA)–gelatin (Ge) composite microgels was investigated for use in treating vocal fold injury and scarring. Cell adhesion integrins and kinematics of cell motion were investigated in two- and three-dimensional culture conditions, respectively. Human vocal fold fibroblast (hVFF) cells were seeded on HA–Ge microgels attached to a HA hydrogel thin film. The results showed that hVFF cells established effective adhesion to HA–Ge microgels through the ubiquitous expression of β_1 integrin in the cell membrane. The microgels were then encapsulated in a three-dimensional HA hydrogel for the study of cell migration. The cells within the HA–Ge microgel-reinforced composite hydrogel (MRCH) scaffold had an average motility speed of 0.24±0.08 μm/minute. The recorded microscopic images revealed features that are presumably associated with lobopodial and lamellipodial cell migration modes within the MRCH scaffold. Average cell speed during lobopodial migration was greater than that during lamellipodial migration. The cells moved faster in the MRCH than in the HA–Ge gel without microgels. These findings support the hypothesis that HA–Ge MRCH promote cell adhesion and migration; thereby they constitute a promising biomaterial for vocal fold repair.

* Correspondence should be addressed to Maryam Tabrizian: 3775 University Street, Department of Biomedical Engineering, Faculty of Medicine, McGill University, Montreal, QC, H3A 2B4, Canada. Tel: +1 (514) 398-8129, Fax: +1 (514) 398-7469, maryam.tabrizian@mcgill.ca. Luc Mongeau: Biomechanics Laboratory, Department of Mechanical Engineering, McGill University, 817 Rue Sherbrooke Ouest, Montreal, QC, H3A 0C3, Canada, Tel: +1 (514) 398-2777, Fax: +1 (514) 398-7365, luc.mongeau@mcgill.ca.

Hossein K. Heris: Biomechanics Laboratory, Department of Mechanical Engineering, McGill University, 817 Rue Sherbrooke Ouest, Montreal, QC, H3A 0C3, Canada.

Jamal Daoud: 3775 University Street, Department of Biomedical Engineering, Faculty of Medicine, McGill University, Montreal, QC, H3A 2B4, Canada.

Sara Sheibani: Station Main, Medicine Hat, Biological Threat Defence Section, Defence R&D Canada-Suffield, Medicine Hat, AB, T1A 8K6, Canada.

Hojatollah Vali: Strathcona Anatomy & Dentistry Building, 3640 University Street Montreal, QC, H3A 0C7, Canada.

Supporting Information

Supporting Information is available from the Wiley Online Library or from the author.

Keywords

cell adhesion/spreading; cell migration mechanisms; hyaluronic acid/gelatin hydrogel; vocal fold repair

1. Introduction

Tissue engineering strives to repair or regenerate damaged and diseased tissues through the use of scaffold materials [1]. Three-dimensional biomimetic scaffolds may be utilized to guide cells into injury sites. Specific interactions between cells and their microenvironment are needed to promote cell adhesion, migration, growth, and differentiation, as all these factors are believed to enhance tissue regeneration [2]. One promising strategy involves the injection of bioactive and biodegradable polymers and hydrogels with tailored mechanical properties. From a clinical perspective, this approach is attractive because it has the potential to minimize patient discomfort, limit the risk of infection, limit scar formation, and reduce treatment costs.

Injectable hydrogels have been frequently used for soft tissues such as cartilage [3], vasculature [4], brain [5], and vocal folds [6]. The search for injectable vocal fold biomaterials has largely focused on derivatives of hyaluronic acid (HA) [7, 8], an important extracellular matrix component of the vocal fold lamina propria (VFLP). The VFLP is a very soft connective tissue with a storage shear modulus range of 10–300 Pa at low frequencies (0.1–1 Hz) [9]. The concentration and organization of HA affects tissue stiffness, thereby altering the fundamental phonation frequency [10]. A decrease of HA within the superficial area of the lamina propria is believed to increase the risk of phonotrauma following voice overuse [11]. Previous studies in rabbit animal models have indicated that HA levels were significantly reduced up to 15 days following vocal fold stripping [12], suggesting that local enrichment of HA may be useful for vocal fold repair *in vivo* [13]. However, native HA has a short half-life *in vivo*. Therefore, chemically crosslinked HA hydrogels have therefore been investigated for their potential use in vocal fold scarring treatment because of their longer degradation time [14-17]. Despite potential therapeutic effects as a functional additive to the superficial lamina propria [16, 18], fibroblast cells do not adhere to HA molecules [19]. As for HA, collagen is an important constituent of normal VFLP tissue and serves as a cell adhesion protein. Excessive amounts of collagen in vocal fold tissue results in stiff VFLP tissue, a common disorder referred to as vocal fold scarring. Addition of collagen to HA hydrogels was shown to be advantageous for *in vitro* culturing of vocal fold fibroblasts [20]. Using adipose-derived stem cells and scaffolds for vocal fold augmentation, Park et al. showed that collagen and HA composite scaffolds induce cell proliferation and differentiation [21]. Collagen and HA might also incorporate additional growth factors to guide cell differentiation [22, 23]. Animal-derived collagen may induce some immunogenicity [24]. Collagen crosslinking *in situ* or fibrillation *in vivo* can result in stiff constructs that may not be suitable for vocal fold tissue treatment. Alternatively, gelatin (Ge) is a non-immunogenic, natural biopolymer derived from collagens through controlled denaturation, and it is another useful constituent for fabricating soft HA-based hydrogels. Gelatin contains several amino acid functional groups [25-27] and exhibits biocompatibility,

biodegradation, and cell adhesion properties. Either in a chemically modulated form or blended with other biopolymers, Ge has been widely used for wound and burn dressings, surgical treatments, and for the tissue engineering of bone, skin, and cartilage [28-31].

The aforementioned natural biopolymers generally need to be crosslinked to achieve the desired structural integrity, degradation time, and stiffness. A highly crosslinked network is required to achieve lower degradation rate. While crosslinking significantly increases the stiffness of the HA hydrogels, scaffolds that are stiffer than the surrounding native tissue hamper the oscillation of vocal folds and shield the mechanical stress, thereby inhibit proper mechanotransduction during neo-tissue growth. Longer degradation rates often need to be traded off against lower stiffness. The integration of soft HA hydrogels within native tissue may be poor due to their limited contact surface areas. In an attempt to overcome these limitations, heavily crosslinked dense HA–Ge microgels were embedded within a secondary HA hydrogel. The use of dense HA–Ge microgels improves the degradation properties of the scaffold without compromising the porosity and elasticity of the biomaterial. In addition, HA-Ge microgels possess a relatively large contact surface area that may improve tissue integration and facilitate the controlled delivery of therapeutics [32]. Previous studies have shown that the presence of stiffer microgels increases toughness and resistance to mechanical degradation [33]. Interestingly, the macroscale bulk mechanical properties of HA–Ge microgel-reinforced composite hydrogels (MRCH) could possibly be tuned independently through the adjustment of the microgel dimensions or the intermicrogel crosslinking [18].

Despite numerous advantages of HA-Ge microgels, basic VF cellular interactions such as viability, adhesion, and motility needs to been studied to evaluate their potential use for VF tissue engineering. Adhesion of VF cells to the scaffold is essential for subsequent changes in cellular functions such as proliferation, and mechanotransduction [34]. Motility of VF fibroblast cells, which are either recruited from surrounding tissue *in vivo* or seeded inside the MRCH scaffold *in vitro*, is critical for the subsequent reconstruction of a native-like heterogeneous and layered VFLP tissue. However, crosslinked networks often create a physical barrier to cell motility. If not properly tuned, crosslinking can result in the formation of cellular capsule around the scaffold-tissue interface *in vivo*. Matrix elasticity [35], elastic nonlinearity [36], adhesion [36], degradability [35], and porosity [37] are the main determinants of cell migration mode and speed. The concentration of inter-microgel crosslinker regulates porosity and stiffness, and thus was hypothesized to have a strong influence on cell motility.

In the present study, a scaffold material consisting of a doubly crosslinked HA–Ge–polyethylene glycol diacrylate (PEGDA) network with a hierarchical organization was developed (Figure 1). Nearly monodisperse HA–Ge microgels were prepared by crosslinking of chemically-modified HA and Ge molecules within inverse emulsion droplets using a PEGDA homobifunctional crosslinker. Macroscopic MRCHs were then obtained by further crosslinking the microgel with soluble HA macromolecules through the residual functional groups on the microgel surface, using different concentrations of the same PEGDA crosslinker. Immortalized hVFF cells were used as the cell model [39], and cytotoxicity and cell adhesion on HA–Ge microgel substrates were investigated. The

migration kinematics of hVFF cells was studied using immunolocalization and time-lapse imaging techniques within the three-dimensional soft and porous external matrix and, for comparison, in microgel-free (bulk) HA–Ge hydrogels.

2. Results and discussion

2.1. Cytotoxicity of HA–Ge microgels

Figure 2 shows the microgel cytotoxicity results over a culture period of three days. Both the 3HA/1Ge/5PEGDA and the 2HA/2Ge/5PEGDA formulations of HA-Ge microgels promoted significant cell proliferation relative to bare polypropylene surfaces. While neither microgels exhibited any cytotoxicy, cell viability was lower than that observed on poly-L-lysine-coated surfaces. The microgels only covered 10–20% of the culture surface, thus accounting for the limited cell proliferation relative to poly-L-lysine coating, which covered the entire surface of the culture plate.

Cell viability for the 3HA/1Ge/5PEGDA formulation was similar to that for 2HA/2Ge/5PEGDA. However, 3HA/1Ge/5PEGDA had a greater stiffness due to its lower Ge concentration [40]. It was therefore used for the remainder of the current study.

2.2. Cell adhesion on microgels attached to hyaluronic acid hydrogel film

Figure 3a shows a confocal image of the hVFF cells cultured on 3HA/1Ge/5PEGDA microgels crosslinked to the bulk HA thin film (Figure 1c). It was observed that hVFF cells spread effectively on the composite crosslinked substrate. Conversely, the cells adopted a more circular morphology with less spreading in the control samples (HA thin film with no crosslinked microgels) (Figure 3b), which is typical of soft substrates [41]. The control sample contained very few stress fibers, a further indication of poor cellular adhesion. In contrast, the cells cultured on the thin film reinforced with HA–Ge microgels exhibited elongated actin stress fibers associated with cellular adhesion.

The major cellular integrin receptors for collagen and Ge are $\alpha_1\beta_1$, $\alpha_2\beta_1$ [42], and $\alpha_5\beta_1$ [43]; the integrins $\alpha_5\beta_1$ and $\alpha_8\beta_1$ recognize the RGD sequence [44]. Anti-β_1 integrin staining was therefore used to show the location of integrin cell-matrix interactions induced by the attachment of microgels to the elongated cell surface. This is attributed to the expression of β_1 integrin at the cell surface, indicative of hVFF adhesion, and the respective cell interactions with HA–Ge microgels crosslinked to the bulk HA gel.

The distribution of integrins over cell surface and types of the membrane proteins involved in cell adhesion may vary from two- to three-dimensional culture conditions [45]. However, β1 integrin is common in both two- and three-dimensional matrix adhesions [45]. The two-dimensional culture conditions was chosen for showing the existence of ligand-integrin interactions between HA-Ge microgels and hVFF cells because it more facile to stain and image cells on 2D surfaces.

Figure 4 shows a magnified image of an adhered cell. The β_1 integrin is expressed almost ubiquitously in the cell membrane, particularly around the cell periphery. A higher magnification image (insets in Figure 4, dashed arrow) further indicated the co-localization

of β_1 integrin with the cell's actin filaments. The adhesion molecules were greatly expressed where a high amount of actin was also expressed, confirming the importance of adhesion for cell spreading and a robust intracellular structure. These findings are consistent with the literature. Matrix stiffness elicits actin rigidity, which is central to the promotion of cellular adhesion [46]. In several cases, co-localization between HA–Ge microgels and β_1 integrin was identified, suggesting that Ge plays a role in establishing adhesion. Co-localization was more pronounced near the leading edge of the cell, as shown by the white arrows in the inset of Figure 4d.

Orthogonal views of the cells attached to the composite surface were analyzed to identify the relative position of the microgels with respect to the cell's cytoskeleton and nucleus (Figures S1 and S2 in supplementary material). The microgels were surrounded by the actin cytoskeleton at the bottom of the cells. Some microgels were found above the cell membrane; however, no microgel was observed inside the nucleus or inside the cell.

Microgels that were unattached to the HA hydrogel surface did not elicit significant cell spreading or adhesion. It was also observed that the HA–Ge microgel monodispersity on the surface was altered. Thus, these results indicate that the cells were able to move the non-crosslinked microgels instead of anchoring and exhibiting cell-microgel interactions and subsequent adhesion/spreading, as for the crosslinked microgels. This is in line with previous findings indicating an inhibition of cell spreading caused by cell-induced microgel movement [47].

The above results demonstrate that the procedure for microgel crosslinking to the HA molecules was effective and yielded an integrated MRCH network. The microgels remained attached to the substrate despite repeated washing during sample preparation and subsequent cell seeding.

2.3. Cell migration in MRCH

Figure 5 shows a three-dimensional reconstruction of the cells encapsulated inside the composite hydrogel, which were alive and metabolically active at the time of imaging (see movie 1 in supplementary material). Larger microgels were used for the purpose of illustration in this section. The concentrations of cells and microgels might be underestimated due to the adjustment made to the brightness and contrast for enhanced image quality. The microgel shape appears to be oval, which is a common artifact of the three-dimensional construction of confocal microscopy images [48].

Cells attached to the three-dimensional construct of MRCH displayed a mainly spherical phenotype (Figure 5). The cell diameter immediately after culture was 10 μm, increasing to 15–30 μm following 16–24 hours of culture. This increase indicates cytoskeleton reinforcement during culture in the scaffold. Some cells were attached to the microgels at the time of imaging, as shown in Figure 5, whereas others were observed in the external HA network. It could thus be speculated that the cells in proximity of the microgels at the time of encapsulation could easily locate and attach to the respective microgel substrates. The cells further from the microgels were viably observed in the external HA matrix at the time of imaging.

It is well accepted that cells migrate inside the scaffold in response to chemical or mechanical gradients [49]. Based on observations, it is apparent that the cells migrated or oscillated in random directions. Because the microgels were distributed isotropically inside the composite gel scaffold and no drug/growth factor was encapsulated within the microgels, only the cells in close proximity moved towards the microgels as demonstrated in supplementary material Figure S3. This is attributed to the process of mechanotaxis, in which cells sense the elasticity gradient induced by the microgels and migrate toward stiffer regions [50-53].

The cells attached to the microgels exhibited a lower motility than the cells in the external matrix did. Figure 6 shows a fast-moving cell inside the scaffold. The speed varied from v_c=1.7±0.5 μm/minute (μm/min) during the first 45 minute to v_c=0.4±0.1 μm/min during the last stage of migration, when the cell was oscillating mostly due to the elastic deformation of the matrix and the hydraulic pressure inside the cell.

Cell speed was assessed for different crosslinker concentrations, as this was the main parameter in controlling the mesh size and elasticity of the HA–Ge matrices. Table 1 summarizes the average speed of ten randomly selected cells over a period of 3 to 6 hours for two different microgel size distributions. As shown in Table 1, the fabricated MRCHs are very soft, with shear storage modulus less than 200 Pa, and thus they are injectable. The MRCHs after being fully cured could be easily injected through a 25-gauge needle. Crosslinker concentrations of 0.25%–0.50% w/v constituted the external network of the MRCH biomaterials used for migration assays. Both crosslinker concentrations in the external network (0.25% and 0.50% w/v) were about two orders of magnitude lower than the crosslinker concentration in the dense internal network of HA–Ge microgels. The cell speed was much greater within the loosely crosslinked composite gel than in the gel with higher crosslinker concentration in the external network for both microgel size distributions. Moreover, the cell speed in the network with greater crosslinking had a lower standard deviation than that in the loosely crosslinked network.

Time-lapse light microscopy experiments were therefore performed to elucidate the high variation in cell speed inside the composite gel with a loose external network (0.25% w/v PEGDA crosslinker). Lobopodial and lamellipodial migration modes, common in non-cancerous fibroblast cells [54], were identified for the MRCH (see movie 2 in supplementary material). Lobopodial and lamellipodial modes were distinguished by their clear differences in the morphological characteristics of the cell's leading edge [55], as shown in Figures 7 and 8. Fibroblast cells can adapt and switch modes within various matrices to ensure efficient cell migration [56]. In lobopodial mode, they are usually identified by blebs around the cell [36]. Lobopodia are intracellular hydrolytic pressure-driven protrusions [57] that aid cell deformation of the surrounding extracellular matrix and facilitate migration. Lamellipodia are extensions of the cytoplasm in the leading edge of many migrating cells. These extensions are driven by actin polymerization.

Lobopodial migration velocities of the hVFFs were greater than lamellipodial migration velocities. Excluding the low speed periods of cell movement, the greatest migration speeds measured at the leading edges of the cells were v_c=2.1±0.5 μm/min, and v_c=0.6±0.2 μm/min

for lobopodial and lamellipodial motion, respectively. Blunt cylindrical protrusions and lateral blebs, the main physical characteristics of lobopodia, were observed in the first 35 minutes of lobopodial cell migration (Figure 7). Under physiological conditions, this mode of migration has been reported for cells inside the dermis [36]; it is not yet known whether cells perform matrix proteolysis in this mode [58]. It has also been reported that normal (non-cancerous) fibroblast cells can alternate between lobopodia- and lamellipodia-based migration mechanisms [36]. Both mechanisms are more or less dependent on cell-matrix adhesion [55], and therefore, involve integrin-based interaction of the cells with the MRCH microenvironment.

2.4. Cell migration within HA–Ge hydrogels with no microgels

Since the distance between large microgels in the composite gel was on the order of the cell diameter, and the cells attached to the microgels had a low motility, it seems plausible that the external HA matrix plays the greatest role in cell migration, at least for composite gels with large HA–Ge microgels. The effect of the biophysical properties of elasticity and porosity, as well as the biochemical property of adhesion molecules on cell migration and speed, are shown in Tables 1 and 2. Because the external HA matrix is a very soft, porous and loose structure, direct measurement of the porosity was not possible using scanning electron microscopy. Therefore we chose to speculate porosity qualitatively using numerical values between 1 (low porosity) and 5 (high porosity), based on the concentration of the constituents.

Table 2 shows the speeds of cells in microgel-free HA–Ge bulk hydrogels at varying concentrations of constituents. According to these results, increasing the crosslinker density significantly decreased cell speed inside the bulk gel. But, adding Ge to the HA matrix did not significantly change the average cell speed. While it is known that greater adhesion might increase cell contractility and speed during lamellipodia-based migration [36]. In another set of migration experiments, the crosslinking density of the bulk HA–Ge was lowered to 0.25% w/v in order to draw a comparison with a bulk HA with 0.25% w/v crosslinker. The speed of the cells was relatively lower in the HA– Ge bulk gel (v_c=0.09±0.04 μm/min) than in the HA bulk gel (v_c=0.15±0.07 μm/min), suggesting that lobopodia-based migration might be more prominent in the matrices with low adhesion properties. The speed of cells in MRCH with submicron HA–Ge microgels (v_c=0.24±0.08 μm/min) is significantly greater than the HA–Ge hydrogel (v_c=0.09±0.04 μm/min). One could conclude that adding Ge in the form of dense microgels with a discrete distribution in the HA matrix offers more efficient cell migration than adding Ge molecules with a uniform distribution in the HA matrix (Tables 1 and 2). These results are in line with recent findings. It was previously shown that a high local ligand density and a low global ligand density is more effective in inducing adhesion and spreading than a low local ligand density with higher global ligand density [59]. It has also been shown that cells are more motile on a substrate with localized adhesion points than one with uniform adhesion points due to the limited focal adhesion growth size [60, 61]. The focal adhesion size is similar to the microgel size, as shown in Figure 4. Therefore, microgels limit the growth in size of focal adhesions. Although focal adhesions are necessary for the adhesion of cells to extracellular matrix and mechanotransduction, strong focal adhesion reduces cell migration speed [62].

Comparing rheological data for MRCH and HA-Ge hydrogels, the addition of Ge in the form of HA–Ge microgels overall elastic modulus of the matrix. According to our previous measurements using an atomic force microscope, the Young's modulus of HAGe microgels is 22±2.5 kPa [32]. Assuming that HA–Ge microgels are isotropic and incompressible (Poisson's ratio = 0.5), the storage modulus of the microgels would be 7.3 kPa. The HA hydrogel with no microgel had a storage modulus of 23±9 Pa, whereas MRCH had a storage modulus of 88±23 Pa. This clearly indicates that HA–Ge microgels reinforced the stiffness of the composite hydrogels. When Ge was simply crosslinked to the HA network, the overall elastic modulus and porosity were even lower (23±9 Pa). However, no significant change in cell motility was observed between HA–Ge hydrogels with different Ge concentrations. This might be because a softer matrix supports better motility, while lower porosity hinders cell motility.

The density of the crosslinker affects porosity and elastic modulus. By comparing the data in Tables 1 and 2, it is also evident that the elastic modulus of the bulk matrix did not significantly affect cell migration speed, despite some correlation in the data presented in Table 2. Therefore, the findings of our work suggest that a combination of matrix elasticity, porosity, and integrin-based interactions between cells and dense HA–Ge microgels influence cell motility in the MRCH matrix.

It has recently been shown that the non-linearity of matrix elasticity is the main factor in determining the mode of cell migration in the matrix [36]. Cells within linearly elastic matrices adopt lobopodia-based migration, whereas in non-linearly elastic matrices, such as collagen gels, cells tend to migrate through a lamellipodia-based mechanism [36]. Indeed, the analysis of elastic behavior of HA–Ge hydrogels (Figure S4) indicated that HA-based hydrogels are linearly elastic over a wide range of strains (0.7–1). According to recent findings [36], lobopodia-based migration seems to be the mechanism of choice inside HA-based bulk and composite gels. However, both lobopodial and lamellipodial mechanisms coexist for HA-based gels. While the greater pore size promotes lobopodial locomotion, matrices with a lower porosity promote the lamellipodial mechanism. We speculate that the low mesh size of the prepared matrix did not allow for such a transition to occur.

The motility of cells inside the bulk HA hydrogel with 0.25% w/v crosslinking was vc=0.15±0.07 μm/min, similar to that in the composite gel with large microgels but lower than that in the composite gel with submicron microgels, as shown in Tables 1 and 2. Although lobopodial migration is promoted by linear elasticity, it is still adhesion-dependent because focal adhesion is also present during this mode of migration [58]. We thus speculate that high local ligand density and low global ligand density distribution by microgels increase the speed of both lamellipodial and lobopodial cell migration modes by controlling the size and the strength of focal adhesions.

Future work involving the use of growth factor gradients might reveal more information regarding the mechanisms of fibroblast cell migration inside HA hydrogels. A large cell migration speed can aid cell infiltration from the surrounding tissue and help achieve a uniform distribution following proliferation.

3. Conclusions

Using a cell model of immortalized hVFFs, HA–Ge-based microgels were used to investigate cell viability, adhesion, and migration in a simulated *in vitro* environment. Submicron-sized (mean d_p<1 μm) microgels were found to promote cell adhesion, spreading, and migration. Crosslinking the microgels to an external HA-based network, mimicking extra cellular matrix conditions, had a significant impact on cell adhesion and spreading. The composite hydrogels allowed for greater cell migration speed in the external network as a result of controlling cellular adhesion at the locus of dense microgels. The proposed microgels would thus offer an effective cell substrate medium and potential therapeutic avenue for vocal fold repair and regenerative applications.

4. Experimental Section

4.1 Materials

Thiolated HA (CMHA-S or Glycosil, MN-200 kDa, thiolation: 40% of carboxyl groups), thiolated Ge (Gtn-DTPH or Gelin-S, MN-25 kDa, thiolation: 40% of carboxyl groups), and PEGDA (Mw ≈ 3,400 g mol^{-1}) were purchased from BioTime (Alameda, CA). Dioctyl sulfosuccinate sodium salt or aerosol OT (AOT, 98%), 2,2,4-trimethylpentane (isooctane, anhydrous), 1-heptanol (1-HP), acetone, and isopropyl alcohol were obtained from Sigma–Aldrich (Buchs, Switzerland). Cell proliferation reagent, WST-1 was purchased from BioVision Inc. (San Francisco, CA). A DyLight™ antibody labeling kit was purchased from Thermo Scientific (Milwaukee, WI, USA). The monoclonal antibodies, mouse anti-beta-1 (anti-β_1), and secondary monoclonal antibody against mouse were purchased from Abcam (Cambridge, MA). Vybrant® DiD, Hoechst 33342 and phalloidin dyes were purchased from Molecular Probes (Eugene, OR).

4.2. Fabrication and synthesis of HA–Ge microgels

Microgels were fabricated in two sizes and dispersity ranges: i) small and monodispersed with a diameter (d_p) of 0.5–1 μm; and ii) large and dispersed with a d_p between 1–15 μm. A solution containing 1% thiol-modified HA, 1% thiol-modified Ge, and 5% crosslinker was prepared and sonicated for 30 s for homogeneity. The HA, Ge, and PEGDA crosslinker solution was obtained by first mixing HA and Ge at volumetric ratios (HA/Ge) of 1/3 or 1/2. The PEGDA crosslinker, at a unity volumetric ratio (PEGDA/(HA–Ge)), was then added to the HA/Ge solution for use as the aqueous phase. The mixture was injected into an organic phase consisting of 0.25 M AOT and 0.05 M 1-HP in iso-octane at an organic-to-aqueous phase volume ratio of 15. The solution was stirred at room temperature for 15 minutes at 12,000 rpm and 16,000 rpm to fabricate large and small microgels, respectively. The microgels were repeatedly washed with acetone and isopropyl alcohol, and then centrifuged to remove any excess surfactants and co-surfactants from the surface.

Microgels were sterilized by immersion in 70% ethanol for ten minutes, then centrifuged, dried, re-suspended in sterilized water, and repeatedly rinsed.

4.3. Cytotoxicity measurements using hVFF cell culture

Microgels with constituents concentration of either 3.75 mg HA/1.25 mg Ge/25 mg PEGDA/ml or 2.5 mg HA/2.5 mg Ge/25 mg PEGDA/mL were crosslinked using PEGDA. These formulations are referred to as 3HA/1Ge/5PEGDA and 2HA/2Ge/5PEGDA to reflect the weight ratio of Ge in the HA–Ge mixture before the addition of the crosslinker and the weight ratio of PEGDA to the HA–Ge mixture. The microgels were nearly monodisperse with a diameter varying between 0.5 and 1.5 μm. Microgels were dispersed in 70% ethanol and then poured into a polypropylene 96-well cell culture plate. The ratio of the dry particle weight to the volume of 70% ethanol was 2.5 mg/mL. The samples were dried in a laminar flow culture hood and were rinsed twice with phosphate buffered saline (PBS). Approximately 20% of the plate's surface was covered with the microgels. Poly-L-lysine-coated surfaces and unmodified surfaces were used as positive and negative controls, respectively. Three replicas of each configuration were used for cell seeding. Two more replicas of 3HA/1Ge/5EGDA with no cells were prepared in another plate as a negative control to extract the background auto fluorescence of the microgel.

The cells were incubated in 96-well plates at 37°C in a humidified atmosphere with 5% CO_2 and 95% air. A volume of 10 μL of WST-1 reagent was added to the wells at different time points (day-0, day-1, day-2, day 3). Fresh media was replaced in the wells to remove any dead cells from the solution before adding WST-1 reagent. The cells were further incubated for 90 minutes after the addition of the WST-1 reagent. Subsequently, the supernatant contents of each well were transferred to another well plate for calorimetric analysis. Cell viabilities were monitored over three days by measuring light absorbance at 450–595 nm using a FLX800 microplate reader (Bio-Tek Instruments, Inc., VT, USA).

4.4. Two-dimensional hVFF cell culture with microgels

4.4.1. Immunostaining of the microgels—A DyLight™ antibody labeling kit was used to prepare fluorescently labeled Ge for the fabrication of HA–Ge microgels, using the procedure recommended by the supplier. Briefly, 5 mg of lyophilized HA–Ge microgels were dissolved in 0.5 mL of Borat buffer (0.05 M in PBS). The solution was added to the DyLight™ reagent vial, which was then vortexed gently and inverted a few times. Vials containing the microgels were left in the dark with the reagent for two hours at room temperature, centrifuged again, rinsed with PBS, and centrifuged twice more to remove any unreacted dyes and byproducts. The samples were then observed under a fluorescence microscope (Nikon TE 2000-E; Nikon, Tokyo, Japan) at an excitation wavelength of 350 nm and an emission wavelength of 432 nm.

4.4.2. Preparation of microgels on HA hydrogel films—A thin layer of HA hydrogel was prepared by pouring a 100 μL mixture of 1% HA and 1% PEGDA (w/v) crosslinker into 7 mm-diameter microscopy vials (MatTek Corporation, Ashland, MA). The excess mixture was removed after ten minutes, leaving a very thin layer of ~20 ± 5 μm of mixture on the surface. A 30-minute waiting period followed to ensure completion of the gelation process. Then, 50 μL of the solution (2.5 mg/mL fluorescent-stained microgel in 0.5% (w/v) crosslinker solution) was added to each vial over the thin HA layer. The solution was left to settle for 12 hours to allow slow water evaporation and achieve microgel and bulk

HA gel contact without complete dehydration. The microgels were crosslinked to the bulk gel through excess thiol groups on the microgel surface [32] and then washed repeatedly to remove crosslinker remnants and any unattached microgels. The samples were examined under the microscope to ensure that the microgels were firmly attached to the thin HA film (Figure 1c). A thin HA film without microgel attachment was used as a control. Immortalized hVFF cells with a concentration of 10^5 cells/mL were incubated for 16 hours to assess the cellular adhesion properties of the gels. The cells were then fixed, stained, and imaged.

4.5. Confocal microscopy imaging of cell–microgel adhesion integrin

Following cell culture for 16 hours, the samples were collected and fixed in 10% formalin for 20 minutes. Cell permeabilization was accomplished through incubation in a 0.1% Triton X (w/v) solution for five minutes. The samples were incubated with primary monoclonal antibodies, mouse anti-β_1, overnight at 4°C. They were subsequently incubated with a secondary monoclonal antibody against mouse, conjugated with Cy5 (Abcam) for one hour at room temperature. Following washes with standard PBS with Tween®, the cells were incubated with Hoechst 3422 and Alexa Fluor® 488 phalloidin dyes (Molecular Probes) for 20 minutes to label the cell nucleus and F-actin, respectively.

A Zeiss LSM510 laser-scanning confocal microscope (Zeiss, Oberkochen, Germany) with an oil–immersion Plan-Neofluar (60 × 1.3 NA) objective lens was used to obtain Z-stacks of images in multiple confocal planes. The intervals (z-steps) between the planes were 0.4–0.5 μm, and the total thickness of the imaged volume was 10–15 μm.

4.6. Encapsulation of hVFFs in composite gel for cellular migration

4.6.1. Cell staining and tracking—Vybrant® DiD cell-labeling solution, with an absorbance wavelength of 644 nm and an emission wavelength of 655 nm, was used as a cell membrane fluorescent marker. The cells were trypsinized and collected through centrifugation at 1,500 rpm for five minutes. They were then suspended in PBS at a concentration of 10^6 cells/mL and stained through the addition of 5 μL of labeling solution per 1 mL of suspension. The solution was mixed by gentle pipetting and incubated for 20 minutes at 37°C. The cells were then collected by centrifugation at 1,500 rpm for 5 minutes and suspended in warm cell culture medium. The procedure was repeated three times to remove the labeling molecule remnants from the cell solution before encapsulation in the composite hydrogel-microgel system (Figure 1d).

4.6.2. Encapsulation of stained cells in composite gel—The fluorescently labeled HA–Ge microgels were dissolved in a 0.5% thiolated HA (w/v) solution at a concentration of 5 mg/mL. The microgels were dispersed using a sonicator (44 kHz) for 5 minutes. A solution containing 10^5 stained cells/mL was mixed with an equal volume of the prepared microgels in HA solution, dropping the microgel concentration to 2.5 mg/mL in the final solution. Finally, the PEGDA crosslinker (2.5–5 mg/mL) was added to crosslink the network and encapsulate the cells inside the composite gel. Microgel-free (bulk) hydrogels containing hVFF (10^5 cells/mL), thiol modified HA (0.5% w/v) and different concentration of Ge (0, 0.25, 0.37 w/v) and PEGDA (0.25, 0.37, 0.50 w/v) were also prepared.

4.7. Time-lapse imaging of cell migration

A Zeiss LSM410 confocal laser scanning microscope (CLSM) with a temperature- and CO_2-controlled (37°C, 5% CO_2, respectively) chamber was used to obtain time-lapse images in multiple confocal planes (Z-stacks). The time interval between images was 10–15 minutes over a total imaging time of 4–6 hours. The imaged confocal planes had a surface area of 625×625 μm^2 with intervals (z-steps) of 4–5 μm.

A Nikon Eclipse TE2000U microscope equipped with a temperature- and CO_2-controlled chamber was used to obtain time-lapse images over longer time periods, between 6 and 24 hours. The images were exported to Matlab. Edge detection and image segmentation was used to detect the centroid of the cells and track them over time to calculate cell speed.

4.8. Rheology measurements

A Bohlin CVO 120 controlled stress rheometer (Malvern instrument) was used to measure the elastic shear properties of the gel at room temperature. Parallel plates with a diameter of 40 mm and a gap of 200 μm were used. The distance between the two plates was calibrated before the measurements. The samples were prepared in syringes and injected to completely fill the gap between the plates. The samples were immersed in water in order to prevent dehydration. An amplitude sweep was performed over a wide amplitude range, and corresponding stain-stress curves were obtained.

4.9. Statistical analysis

All experiments were replicated including control and negative condition groups for each condition. Results are expressed as mean±SEM. Statistical significance was determined by a paired Student's *t*-test, when applicable. Differences were considered significant at $P<0.05$.

Supplementary Material

Refer to Web version on PubMed Central for supplementary material.

Acknowledgements

We gratefully thank NCDCD grant R01-DC005788, the Natural Science and Engineering Research Council of Canada (NSERC), M.Tabrizian NSERC discovery grant, Canadian Institute of Health Research (CIHR), and the Fonds Québécois de la recherche sur la nature et les technologies (FQRNT) for their financial support. We would like to thank Professor Susan Thibeault (Division of Otolaryngology–Head and Neck Surgery, University of Wisconsin) for providing us with immortalized hVFF cells.

References

1. Langer R, Vacanti JP. Science. 1993; 260:920. [PubMed: 8493529]
2. Harunaga JS, Yamada KM. Matrix Biology. 2011; 30:363. [PubMed: 21723391]
3. Mekhail M, Tabrizian M. Advanced healthcare materials. 2014; 3:1529. [PubMed: 24616443]
4. Nelson DM, Ma Z, Fujimoto KL, Hashizume R, Wagner WR. Acta biomaterialia. 2011; 7:1. [PubMed: 20619368]
5. Fon D, Al-Abboodi A, Chan PPY, Zhou K, Crack P, Finkelstein DI, Forsythe JS. Advanced healthcare materials. 2014; 3:761. [PubMed: 24596339]
6. Duflo S, Thibeault SL, Li W, Shu XZ, Prestwich GD. Tissue engineering. 2006; 12:2171. [PubMed: 16968158]

7. Thibeault SL. Current opinion in otolaryngology & head and neck surgery. 2005; 13:148. [PubMed: 15908811]
8. Hirano S. Current opinion in otolaryngology & head and neck surgery. 2005; 13:143. [PubMed: 15908810]
9. Chan RW, Titze IR. The Journal of the Acoustical Society of America. 1999; 106:2008. [PubMed: 10530024]
10. Chan RW, Gray SD, Titze IR. Otolaryngology--head and neck surgery : official journal of American Academy of Otolaryngology-Head and Neck Surgery. 2001; 124:607. [PubMed: 11391249]
11. Butler JE, Hammond TH, Gray SD. The Laryngoscope. 2001; 111:907. [PubMed: 11359176]
12. Gray SD, Titze IR, Chan R, Hammond TH. The Laryngoscope. 1999; 109:845. [PubMed: 10369269]
13. Thibeault SL, Klemuk SA, Smith ME, Leugers C, Prestwich G. Tissue engineering. Part A. 2009; 15:1481. [PubMed: 19072088]
14. Leach JB, Schmidt CE. Biomaterials. 2005; 26:125. [PubMed: 15207459]
15. Arimura H, Ouchi T, Kishida A, Ohya Y. Journal of biomaterials science. Polymer edition. 2005; 16:1347. [PubMed: 16370238]
16. Borzacchiello A, Mayol L, Garskog O, Dahlqvist A, Ambrosio L. Journal of materials science. Materials in medicine. 2005; 16:553. [PubMed: 15928871]
17. Jia X, Colombo G, Padera R, Langer R, Kohane DS. Biomaterials. 2004; 25:4797. [PubMed: 15120526]
18. Jia X, Yeo Y, Clifton RJ, Jiao T, Kohane DS, Kobler JB, Zeitels SM, Langer R. Biomacromolecules. 2006; 7:3336. [PubMed: 17154461]
19. Seidlits SK, Drinnan CT, Petersen RR, Shear JB, Suggs LJ, Schmidt CE. Acta Biomaterialia. 2011; 7:2401. [PubMed: 21439409]
20. Hahn MS, Teply BA, Stevens MM, Zeitels SM, Langer R. Biomaterials. 2006; 27:1104. [PubMed: 16154633]
21. Park H, Karajanagi S, Wolak K, Aanestad J, Daheron L, Kobler JB, Lopez- Guerra G, Heaton JT, Langer RS, Zeitels SM. Tissue engineering. Part A. 2010; 16:535. [PubMed: 19728785]
22. Na K, Kim S, Woo DG, Sun BK, Yang HN, Chung HM, Park KH. Journal of biomedical materials research. Part A. 2007; 83:779. [PubMed: 17559114]
23. Ibrahim S, Ramamurthi A. Journal of tissue engineering and regenerative medicine. 2008; 2:22. [PubMed: 18265428]
24. Lynn A, Yannas I, Bonfield W. Journal of Biomedical Materials Research Part B: Applied Biomaterials. 2004; 71:343.
25. Liu Y, Shu XZ, Gray SD, Prestwich GD. Journal of biomedical materials research. Part A. 2004; 68:142. [PubMed: 14661259]
26. Chang MC, Ko CC, Douglas WH. Biomaterials. 2003; 24:3087. [PubMed: 12895581]
27. Lee SB, Jeon HW, Lee YW, Lee YM, Song KW, Park MH, Nam YS, Ahn HC. Biomaterials. 2003; 24:2503. [PubMed: 12695077]
28. Balakrishnan B, Mohanty M, Umashankar PR, Jayakrishnan A. Biomaterials. 2005; 26:6335. [PubMed: 15919113]
29. Mao J, Zhao L, De Yao K, Shang Q, Yang G, Cao Y. Journal of biomedical materials research. Part A. 2003; 64:301. [PubMed: 12522817]
30. Ciper M, Bodmeier R. International journal of pharmaceutics. 2005; 303:62. [PubMed: 16111845]
31. Li J, He A, Zheng J, Han CC. Biomacromolecules. 2006; 7:2243. [PubMed: 16827594]
32. Heris HK, Rahmat M, Mongeau L. Macromolecular bioscience. 2012; 12:202. [PubMed: 22147507]
33. Shull KR. Nature. 2012; 489:36. [PubMed: 22955605]
34. Anselme K. Biomaterials. 2000; 21:667. [PubMed: 10711964]
35. Ehrbar M, Sala A, Lienemann P, Ranga A, Mosiewicz K, Bittermann A, Rizzi SC, Weber FE, Lutolf MP. Biophysical Journal. 2011; 100:284. [PubMed: 21244824]

36. Petrie RJ, Gavara N, Chadwick RS, Yamada KM. Journal of Cell Biology. 2012; 197:439. [PubMed: 22547408]
37. Schuldt A. Nature Reviews Molecular Cell Biology. 2013; 14:462.
38. Shu XZ, Liu Y, Palumbo F, Prestwich GD. Biomaterials. 2003; 24:3825. [PubMed: 12818555]
39. Chen X, Thibeault SL. Tissue Engineering Part C: Methods. 2008; 15:201. [PubMed: 19108681]
40. Kazemirad S, Heris HK, Mongeau L. Journal of Biomedical Materials Research Part B: Applied Biomaterials. 2015
41. Yeung T, Georges PC, Flanagan LA, Marg B, Ortiz M, Funaki M, Zahir N, Ming W, Weaver V, Janmey PA. Cell Motility and the Cytoskeleton. 2005; 60:24. [PubMed: 15573414]
42. Ivaska J, Heino J. Cellular and Molecular Life Sciences. 2000; 57:16. [PubMed: 10949578]
43. Geiger B, Bershadsky A, Pankov R, Yamada KM. Nature Reviews Molecular Cell Biology. 2001; 2:793. [PubMed: 11715046]
44. Takagi J. Biochemical Society Transactions. 2004; 32:403. [PubMed: 15157147]
45. Cukierman E, Pankov R, Stevens DR, Yamada, K. M. KM. Science. 2001; 294:1708. [PubMed: 11721053]
46. Mason, B.; Califano, J.; Reinhart-King, C. Matrix Stiffness: A Regulator of Cellular Behavior and Tissue Formation. In: Bhatia, SK., editor. Engineering Biomaterials for Regenerative Medicine. Springer; New York: 2012. p. 19
47. Geiger B, Yamada KM. Cold Spring Harbor perspectives in biology. 2011:3.
48. Cole RW, Jinadasa T, Brown CM. Nature Protocols. 2011; 6:1929. [PubMed: 22082987]
49. Singh M, Berkland C, Detamore MS. Tissue Engineering - Part B: Reviews. 2008; 14:341. [PubMed: 18803499]
50. Harland B, Walcott S, Sun SX. Physical Biology. 2011:8.
51. Vincent LG, Choi YS, Alonso-Latorre B, del Álamo JC, Engler AJ. Biotechnology Journal. 2013
52. Wu J, Mao Z, Tan H, Han L, Ren T, Gao C. Interface Focus. 2012; 2:337. [PubMed: 23741610]
53. Tse JR, Engler AJ. PLoS ONE. 2011:6.
54. Petrie RJ, Yamada KM. At the leading edge of three-dimensional cell migration. 2013
55. Petrie RJ, Yamada KM. Journal of cell science. 2012; 125:5917. [PubMed: 23378019]
56. Friedl P, Wolf K. Journal of Cell Biology. 2010; 188:11. [PubMed: 19951899]
57. Yanai M, Kenyon CM, Butler JP, Macklem PT, Kelly SM. Cell Motility and the Cytoskeleton. 1995; 33:22. [PubMed: 8824731]
58. Sixt M. Journal of Cell Biology. 2012; 197:347. [PubMed: 22547405]
59. Deeg JA, Louban I, Aydin D, Selhuber-Unkel C, Kessler H, Spatz JP. Nano letters. 2011; 11:1469. [PubMed: 21425841]
60. Slater JH, Boyce PJ, Jancaitis MP, Gaubert HE, Chang AL, A. L. Markey MK, Frey W. ACS applied materials & interfaces. 2015; 7:4390. [PubMed: 25625303]
61. Eugene WL. RSC Advances. 2014; 4:31581.
62. Kim DH, Wirtz D. The FASEB Journal. 2013; 27:1351. [PubMed: 23254340]

Investigation of the Viability, Adhesion, and Migration of Human Fibroblasts in a Hyaluronic Acid/Gelatin Microgel-Reinforced Composite Hydrogel for Vocal Fold Tissue Regeneration

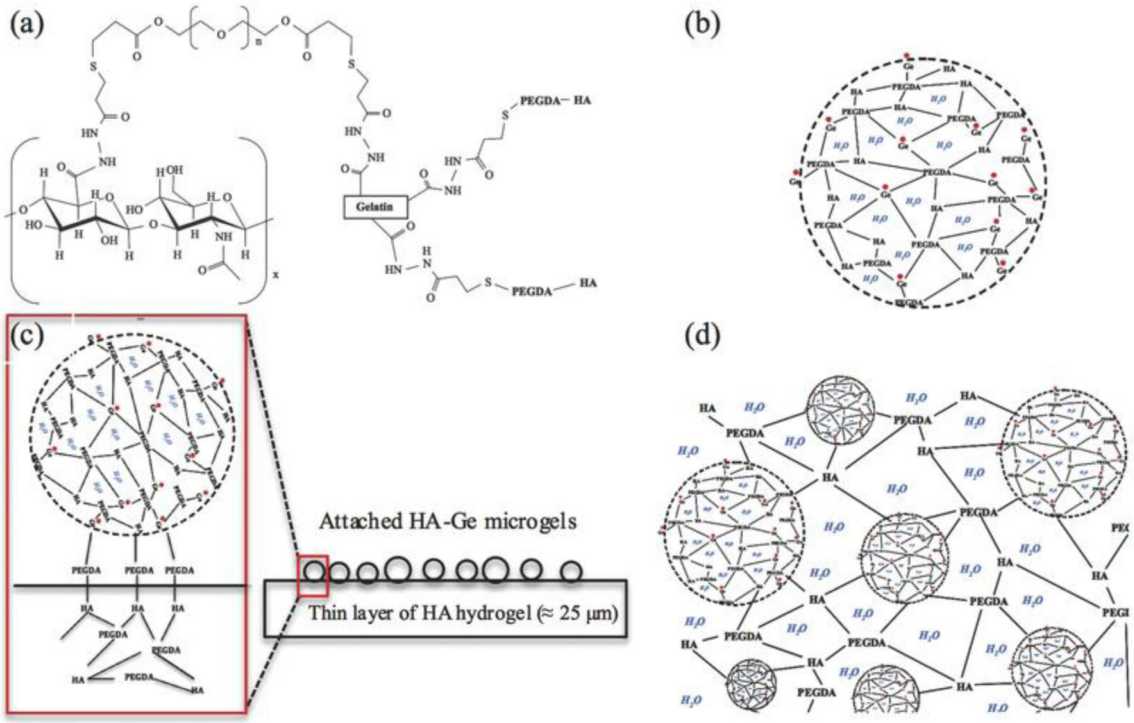

Figure 1.

(a) Schematic of thiol modified HA and Ge cross-linked by PEGDA [38]. (b) Microparticle of cross-linked HA and Ge. (c) Cross-section view of two-dimensional network of HA–Ge microgels attached to thin layer of HA hydrogel. (d) Cross-section view of three-dimensional encapsulation of HA–Ge microgels inside HA hydrogel.

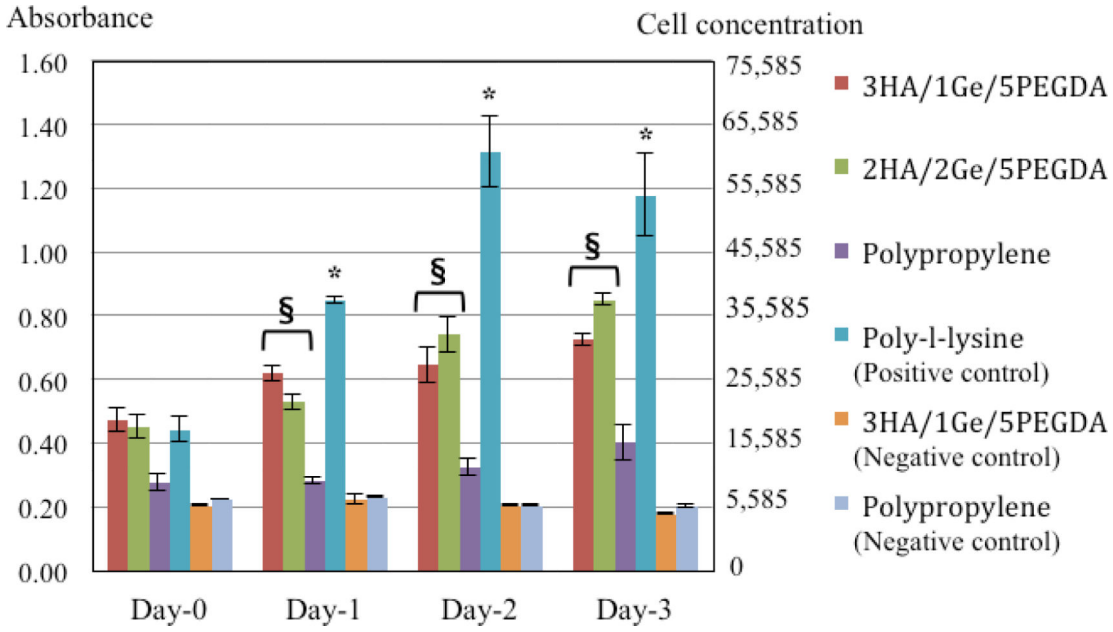

Figure 2.

Cytotoxicity following hVFF culture on microgels over a period of three days. As shown, both the 3HA/1Ge/5PEGDA and 2HA/2Ge/5PEGDA formulations promote significant cell proliferation and activity relative to the cells cultured on uncoated polypropylene surfaces. The measured cellular activity was however lower than that observed on poly-l-lysine tissue culture coated surfaces. There is no statistical difference in cellular proliferation between 3HA/1Ge/5PEGDA and 2HA/2Ge/5PEGDA formulations (n=3, mean ± Standard Deviation, *P and §P<0.05 versus other negative control surfaces). Negative controls of 3HA/1Ge/5PEGDA microgels with no cell seeding confirm the absence of any particle auto-fluorescence.

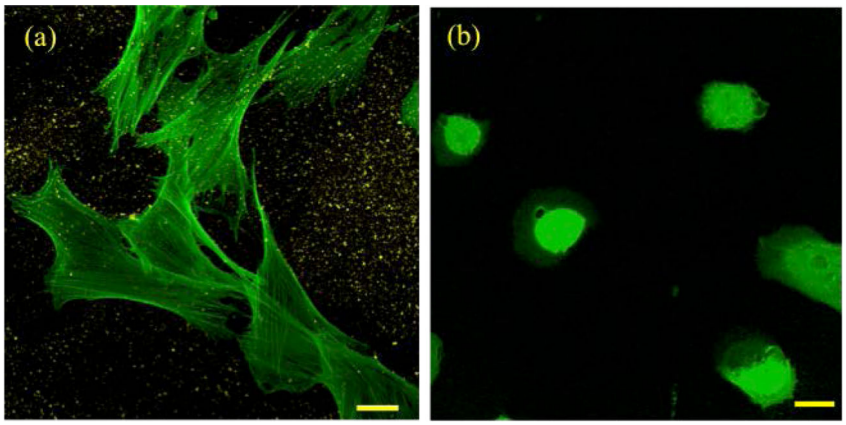

Figure 3.

(a) F-actin expression (in green) of cells cultured on thin HA film with HA–Ge microgels (in yellow). (b) F-actin expression on HA thin film without microgels (control sample). Cells possess circular morphology with less spreading. Scale bars are 25 μm.

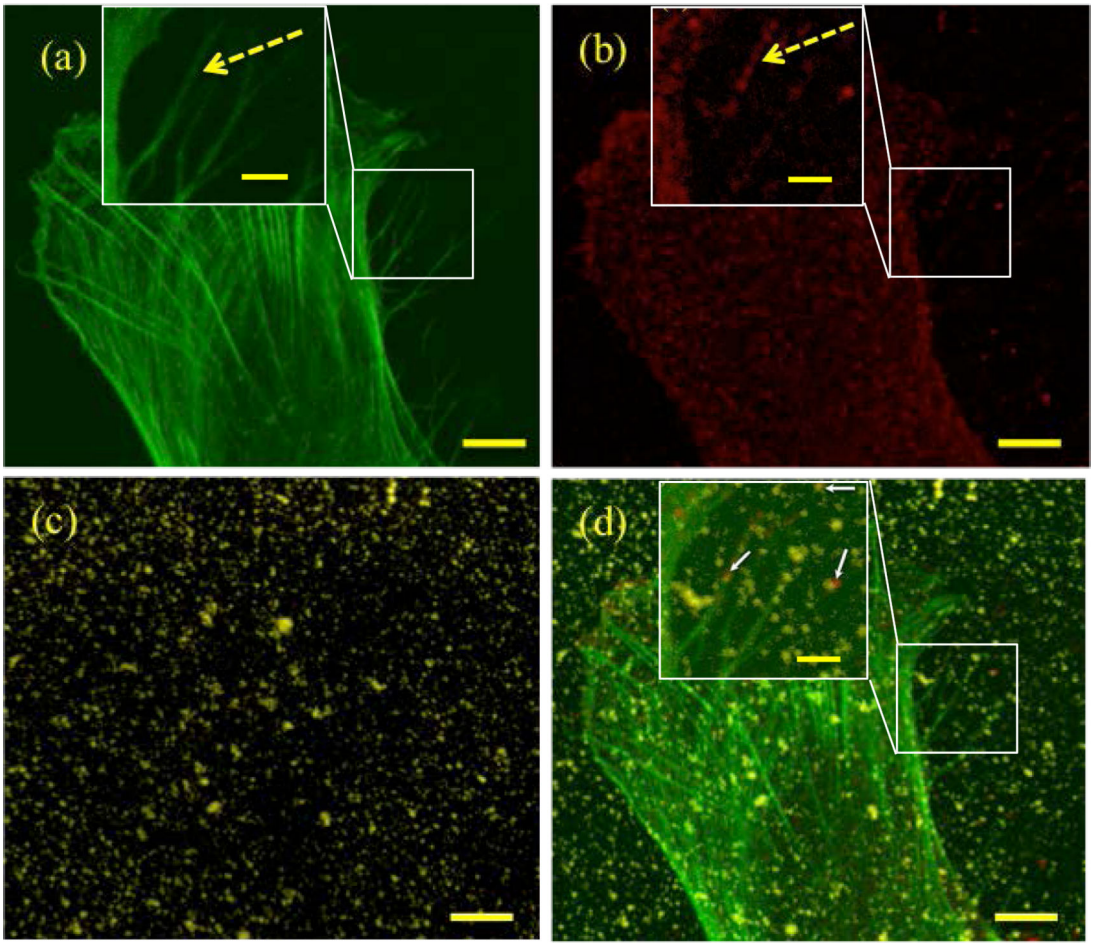

Figure 4.

A focused image of an adhered cell showing (a) F-actin filaments (green) (b) anti-beta integrin (red) (c) nearly monodisperse HA–Ge microgels with size of around 0.5 μm (yellow) (c) superimposed image of (a), (b), and (c). The scale bars are 5 μm. The insets show filopodia area of the attached cell. Dashed arrow show the co-localization of actin and antibeta. White arrows with solid line show the co-localized particles with the anti-beta1. The scale bars in the insets are 2 μm.

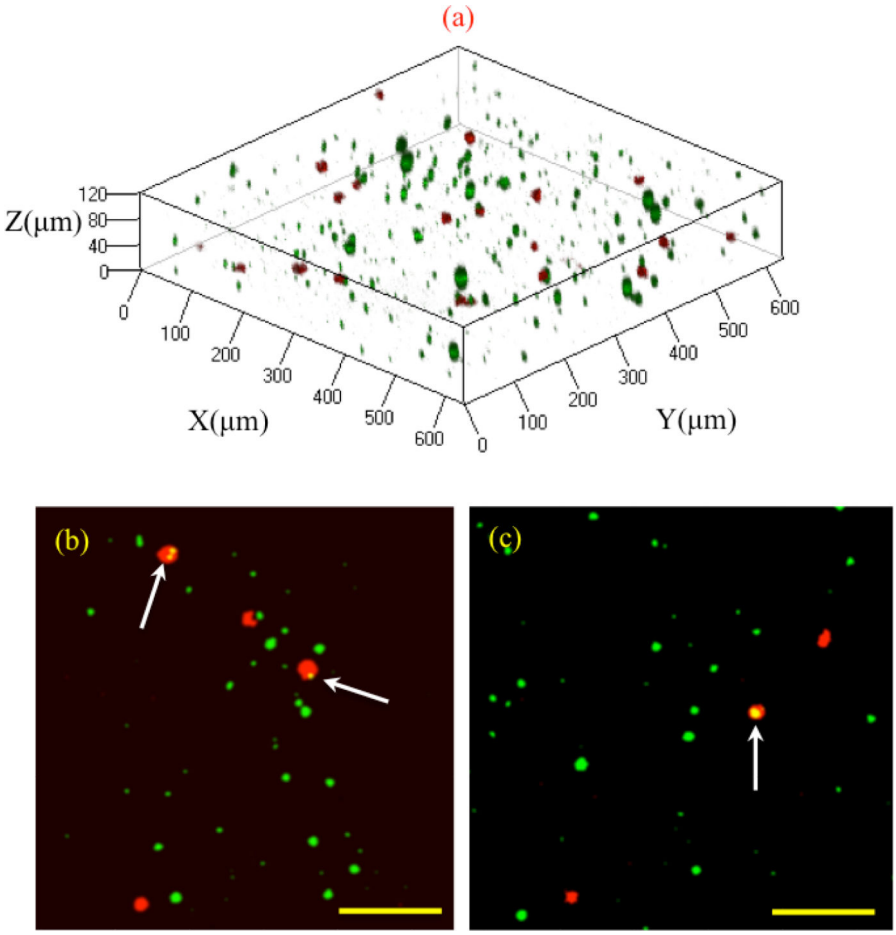

Figure 5.

(a) Cell encapsulation in 3D MRCH network. The cell membrane is shown in red and particles are shown in green. (b), (c) Cell adhesion to a single and multiple particles in 3D shown with white arrows. The scale bar is 120 um.

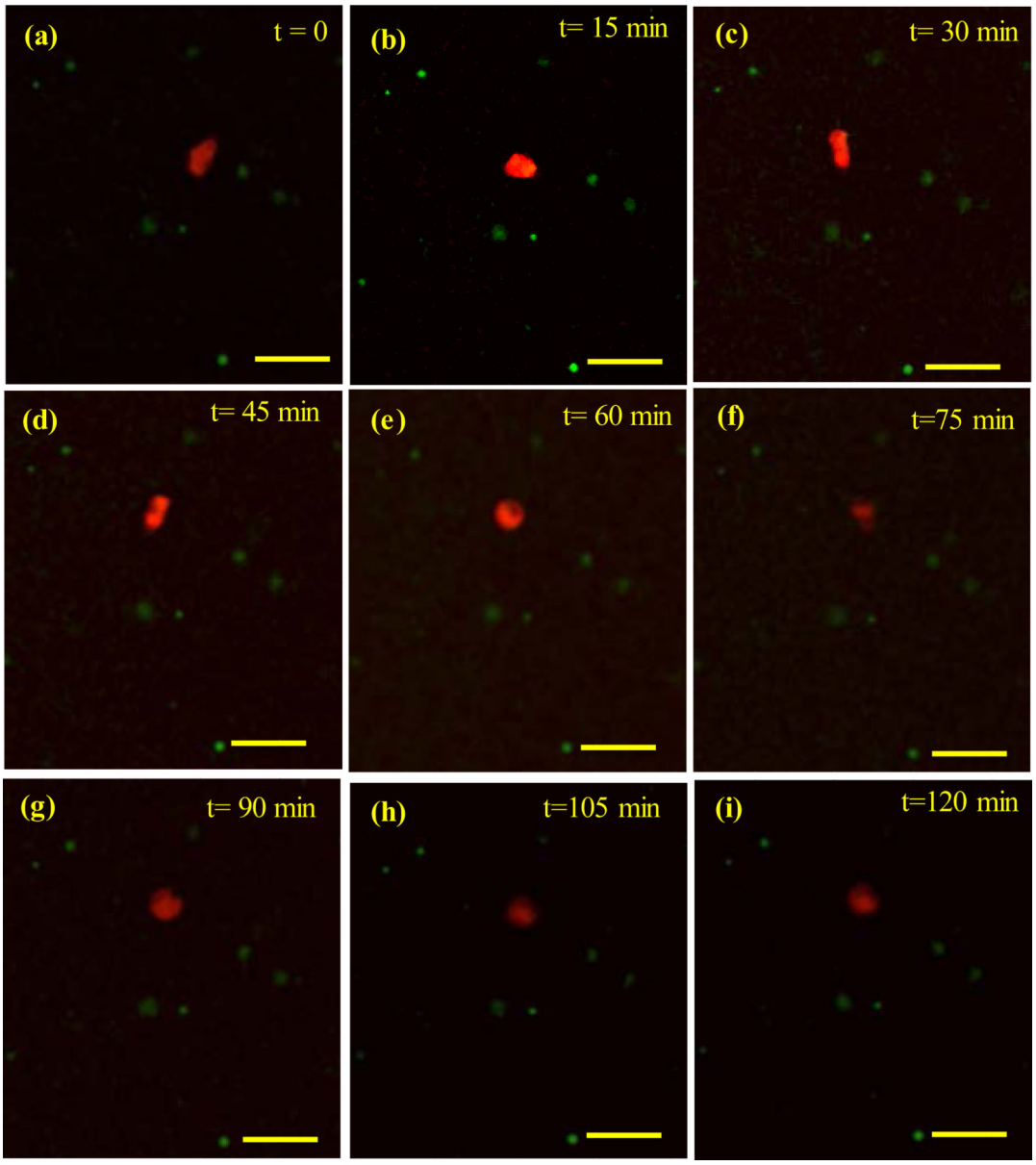

Figure 6.

Fast cell movement in the composite gel. Cell velocity was maximum (v_c=1.7±0.5 μm/min) over the first 45 minutes (a-d). The cell oscillated with a lower velocity of v_c=0.4±0.1 μm/min over the following 75 minutes. Cell was elongated at times t=30, 45 min. Scale bar= 60 μm.

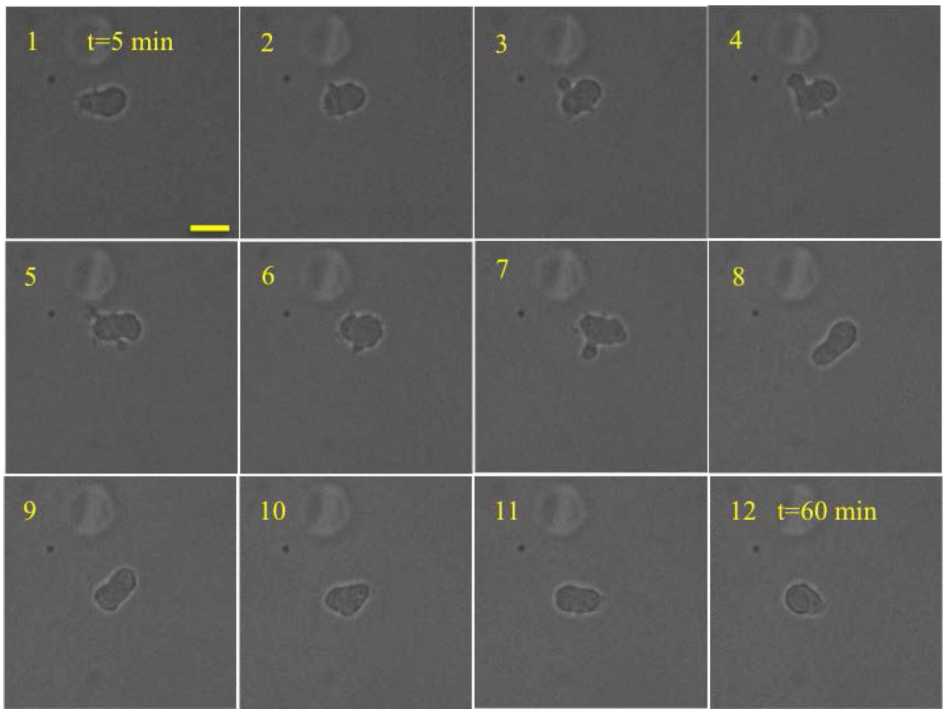

Figure 7.

Lobopodia based cell migration of HVFF inside the scaffold. The interval between the images was 5 min. Scale bar is 20 μm. Lobopodia is shown with white arrow. The average cell velocity at the center of the cell was v_c=0.6±0.4 μm/min. The maximum cell velocity at the leading edge was 2.5 μm/min. The blebs were not seen in the last 25 minutes, which may indicate that the cells had switched to another mode of migration.

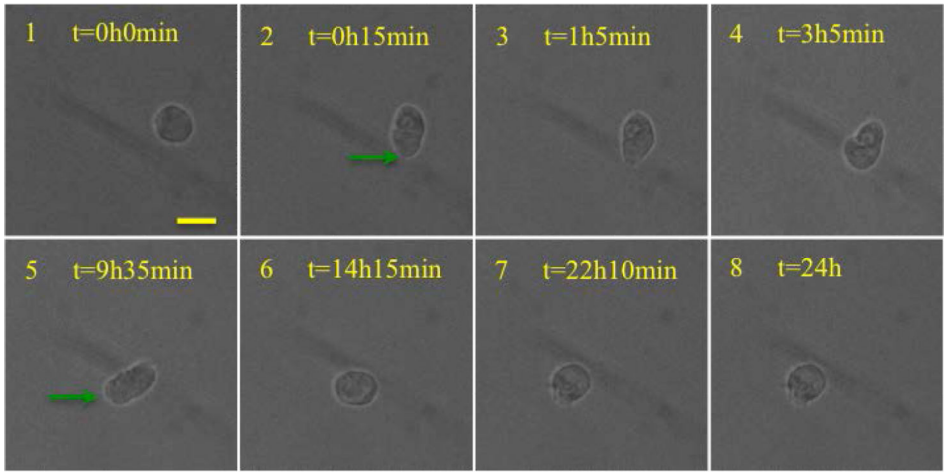

Figure 8.

Images at selected intervals during Lamellipodia based mode of migration inside the scaffold. The average speed of cell center during the period of 24 hours was v_c=0.05±0.02 μm /min. The maximum cell speed at the leading edge was v_c=0.8 μm/min. Possible actin extension in the form of lamellipodia is shown with green arrows. The scale bar is 20 microns.

Table 1

Cell motility velocity (μm/min) inside the composite gel with respect to external network crosslinking concentration. Corresponding shear elastic modulus (Pa) is also provided. Rough estimation of porosity is presented by numbers between 1 (low porosity) and 5 (high porosity). Asterisk indicates statistical significance between pair of data at each row.

Microgel size	**Large microgels (5-15μm)**		**Submicron microgels**	
Crosslinker concentration (%)	0.25	0.5	0.25	0.5
V_c (mean±std)	0.17±0.14	0.06±0.03	0.24±0.08*	0.08±0.04*
Shear modulus (mean±std)	75±15	133±27	88±23*	143±25*
Migration mode	Lamellipodial Lobopodial	Lamellipodial	Lamellipodial Lobopodial	Lamellipodial
Expected porosity	5	1	1	5
Expected cell adhesion	High	High	High	High

Table 2

Cell motility velocity (μm /min) in HA and HA-Ge gels containing no particles. The data is the average of 10 random cells over 24 hours period. Concentrations are shown as percent solution. Elastic shear modulus values are in Pa units. Porosity is qualitatively indicated by numbers between 1 (low porosity) and 5 (high porosity). Cell adhesion is qualitatively indicated using numbers between 1 (low adhesion) and 5 (high adhesion).

Case	1	2	3	4	5	6
HA (%)	0.5	0.5	0.5	0.5	0.5	0.5
Ge (%)	0	0	0	0.5	0.37	0.25
Crosslinker (%)	0.25	0.37	0.5	0.5	0.37	0.25
V_c (mean±std)	0.15±0.07*, †	0.13±0.08	0.05±0.02*	0.06±0.01†	0.07±0.02	0.09±0.04
Mode of migration	Lamellipodial Lobopodial	Lamellipodial Lobopodial	Lamellipodial	Lamellipodial	Lamellipodial	Lamellipodial Lobopodial
Shear modulus (mean±std)	23±9*,‡	66±7#,″	94±11*, #	82±13†,‡	38±8″	18±6†
Expected porosity	5	3	2	1	2-3	3-4
Expected cell adhesion	1	1-2	1-2	5	4	3

The *, †, ‡, and # signs shows statistical significant difference between some pairs of data values.